Failure of film formation of viscoelastic fluid: Dynamics of viscoelastic fluid in a partially filled horizontally rotating cylinder

Yutaka Sumino*
Faculty of Education, Aichi University of Education, Kariya 448-8542, Japan

Hiroki Shibayama
Department of Information Physics and Computing, Graduate School of Information Science and Technology, The University of Tokyo, Tokyo 113-8656, Japan

Tetsuo Yamaguchi
Research Center for Advanced Biomechanics, Kyushu University, Fukuoka 819-0395, Japan

Tadashi Kajiya
Laboratoire Matière et Systèmes Complexes, UMR CNRS 7057, Université Paris Diderot, 10 rue Alice Domon et Léonie Duquet, 75205 Paris Cedex 13, France

Masao Doi†
Department of Applied Physics, School of Engineering, The University of Tokyo, Tokyo 113-8656, Japan
(Received 6 November 2010; published 19 April 2012)

The dynamics of a viscoelastic Maxwell fluid is studied in a partially filled cylinder rotating around a horizontal axis. At low rotational velocity, the fluid behaves in the same manner as a viscous fluid. A thin fluid film is pulled up from the edge of a fluid bump at the bottom of the cylinder, and it covers the inner wall of the cylinder completely. As a result, a steady state is the coexistence of the film and the bump of the fluid. When the rotational velocity of the cylinder is increased, the film formation fails and the bump of fluid rolls steadily at the bottom of the cylinder. This failure of film formation has never been observed in the case of a viscous fluid. At higher rotational velocity, the bump of the fluid starts to oscillate at the bottom of the cylinder. Then, the fluid bump again rolls steadily with a further increase in the rotational velocity. The failure of film formation is explained in terms of the elastic behavior of the viscoelastic fluid near the boundary between the film and the bump regions. The theoretical prediction shows good agreement with the experimental results. We further estimate the condition for which a viscoelastic fluid displays dynamically nonwetting behavior; i.e., the absence of fluid film at any value of rotational velocity.

DOI: 10.1103/PhysRevE.85.046307 PACS number(s): 47.20.Gv, 47.15.gm, 83.80.Qr

I. INTRODUCTION

Wetting is a commonly observed phenomenon in our daily life. Nevertheless, its study presents many challenging problems [1]. Contact line dynamics is one of these challenging problems. When depositing a sample fluid on a solid substrate, a contact line appears that is a coexistence line between the air, the solid substrate, and the sample. When the sample moves on a solid substrate, the shear rate inside of the sample diverges near the contact line. If the sample is a purely viscous Newtonian fluid, the dissipation rate diverges as the shear rate diverges. Thus, the resistance force of the contact line determines the motion of the sample on the solid substrate. However, the application of the above analysis is not trivial when the sample is a non-Newtonian fluid. This is because a non-Newtonian fluid changes its response depending on the shear rate. Despite such inherent difficulties, understanding the contact line dynamics of a non-Newtonian fluid is relevant to the handling of industrial processes such as printing and coating.

Contact line dynamics has been studied a lot over the past few decades [1–3]. With respect to the present work, one can mention several studies about coating flows [4–6] or the shape evolution of droplets sliding down an incline [7–10]. An equivalent of contact line dynamics has also been investigated for a rubbery material moving down on a solid, which occurs during the debonding of adhesives [11–14], and for sliding friction, where the contact line is defined for the boundary of debonded and contact regions. However, there are very few studies on the intermediate case, in which a viscoelastic fluid flows on a solid substrate, with the exception of a few pioneering works [15–17]. In this case, it is expected that the possible transition from liquid to solid will dramatically affect the dynamics of contact lines where the shear rate diverges.

In this work, we study the dynamics of the contact line of a viscoelastic fluid with a hollow cylinder, which is a setup used in earlier works [18–21]. The setup is shown in Fig. 1: the hollow cylinder is partially filled with the sample fluid and rotated about the horizontal axis. This setup avoids the problem of evaporation and is suitable for the observation of contact line dynamics in steady conditions.

In order to study how viscoelasticity affects contact line dynamics, we first compared two types of samples: purely viscous fluids and viscoelastic fluids with similar viscosity.

*ysumino@auecc.aichi-edu.ac.jp
†Present address: Toyota Physical and Chemical Research Institute, Nagakute 480-1192, Japan.

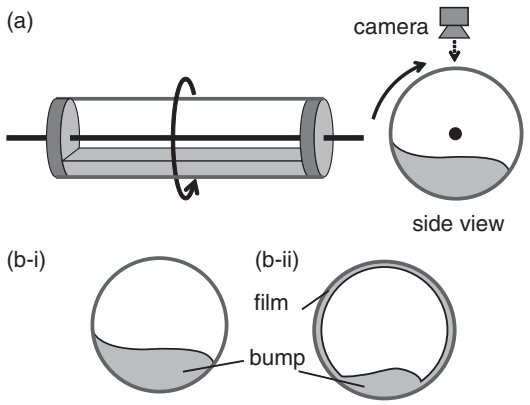

FIG. 1. (a) Schematic representation of the experimental setup. (b) Cross section of the cylinder with a sample. The fluid can be classified into bump and film regions.

As the purely viscous fluid, we used an aqueous solution of polyethylene glycol (PEG) having low molecular weight. As the viscoelastic fluid, we used an aqueous solution of cetyltrymethylammonium bromide (CTAB) and sodium salicylate (NaSal). This aqueous solution is known as an ideal viscoelastic fluid described by the Maxwell model with a single relaxation time [22–25]. We found that the dynamics of wetting and dewetting of these two fluids are quite different from each other. In the case of the aqueous solutions of PEG (viscous fluids), the solution wets the inner wall of the cylinder and forms a stable film above a certain rotational velocity. In the case of the aqueous solution of CTAB and NaSal (viscoelastic fluids), a stable film could not be observed above another critical rotational velocity. We then conducted experiments with viscoelastic samples having different shear moduli and relaxation times over a broad range. Our experiments indicate that the different dewetting behavior in viscoelastic samples arises from the viscoelastic effect occurring near a contact line.

II. EXPERIMENT

The experiment was conducted using the setup shown in Fig. 1. A volume of 300 ml of the sample was placed in a hollow acrylic cylinder, whose radius and length were 40 and 500 mm, respectively. The volume filling fraction of the sample in the cylinder was approximately 12%. The cylinder was rotated about the horizontal axis with a fixed velocity. As the rotational velocity, we measured the velocity of the inner wall of the cylinder, V. V varied from 0.4 to 600.0 mm/s. The fluid behavior was recorded using a CCD camera at 30 frames per second.

For the viscous fluid, we used an aqueous solution of PEG (PEG 6000; Pure Chemical Industries, Ltd.). Solutions with 15, 30, and 60 wt.% concentration were prepared. The shear viscosity and storage modulus of these samples were measured by a Physica MCR-301 (Anton Paar) rheometer (Fig. 2). In order to compare the behavior of the samples with that of viscoelastic fluids, the shear viscosities of samples A, B, and C (Table I) were also measured and are plotted in Fig. 2. The steady viscosities of these viscous and viscoelastic samples were similar [Fig. 2(a)], but the storage moduli were clearly different [Fig. 2(b)], in that the viscous samples only had a negligible storage modulus.

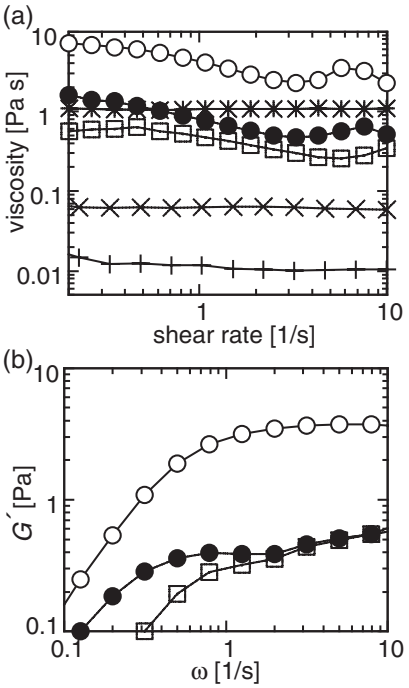

FIG. 2. (a) Steady shear viscosity of viscous fluids (aqueous solution of PEG) [15 wt.% (+), 30 wt.% (×), 60 wt.% (∗)] and that of viscoelastic fluids (aqueous solution of CTAB and NaSal) [A (□), B (•), and C (○)]. The specifications for the CTAB and NaSal solution are given in Table I. (b) Storage modulus of viscoelastic fluids. The symbols are the same as in (a). The storage moduli of the PEG solutions are not shown as they are too small to be plotted on this scale.

For the viscoelastic fluid, we used an aqueous solution of CTAB (Tokyo Chemical Industry) mixed with NaSal (Junsei Chemical). The concentrations of CTAB, i.e., C_d, and that of NaSal, i.e., C_s, were varied, as listed in Table I. Sample E was colored for observation with basic violet 1 (aniline violet), purchased from Tokyo Chemical Industry, whose concentration was 2.5×10^{-4} wt.%. The viscoelasticity of the samples was measured by a Physica MCR-301 (Anton Paar)

TABLE I. Specifications of the viscoelastic samples (aqueous solution of CTAB and NaSal). C_d and C_s represent the concentrations of CTAB and NaSal, respectively. G and τ are the shear modulus and the relaxation time of the samples, respectively.

Label	C_d (mM)	C_s (mM)	G (Pa)	τ (s)
A	10	50		
B	10	20	0.448	4.10
C	25	50	4.69	1.48
D	50	100	16.9	2.19
E	100	100	53.6	2.44
F	80	130	43.5	4.34
G	90	90	48.1	2.01
H	100	150	62.7	4.10
I	110	110	67.3	1.65
J	120	120	77.2	2.16

rheometer, and it was confirmed that the storage modulus and loss modulus fitted the single-mode Maxwell model well, i.e., $G'(\omega)=(G\omega^2\tau^2)/(\omega^2\tau^2+1)$ and $G''(\omega)=(G\omega\tau)/(\omega^2\tau^2+1)$, except in the case of sample A. The fitting parameters, shear modulus G, and relaxation time τ are listed in Table I.

The inner wall of the acrylic cylinder was coated twice with the surface modifier Fluorosurf (FS-1010TH05, Fluoro Technology). The equilibrium contact angles of the aqueous solutions of CTAB and NaSal on the inner wall were from 70° to 90°, whereas those of the aqueous solutions of PEG were from 90° to 105°. In order to avoid transient behavior, data presented here were obtained several minutes after the rotational velocity of the cylinder was set.

III. RESULT

A. Comparison between PEG and CTAB and NaSal solution behaviors

For a typical viscous fluid, it is known that a liquid film is formed on the cylinder surface above a certain characteristic velocity, V_0. For a small equilibrium contact angle, θ_E, V_0 has been estimated as

$$V_0 \sim \frac{1}{9\sqrt{3}l}\frac{\sigma}{\eta}\theta_E^3, \tag{1}$$

where σ is the surface tension of the sample and l is a dimensionless cutoff value that is typically between 15 and 20 [1].

The behavior of the PEG solution in the rotating cylinder was the same as those reported in earlier works [18–21]. When the rotational velocity, V, was lower than the critical velocity V_0 (Table II), the sample did not wet the inner wall of the cylinder; only a fluid bump was observed [Fig. 1(b-i)]. As V approached V_0, the sample gradually wet the inner wall of the cylinder. As V exceeded V_0, the inner wall of the cylinder was completely covered by the sample. There appeared a film of the sample as well as the bump, as shown in Fig. 1(b-ii).

The situation drastically changed for the CTAB and NaSal solution. The film region did not appear [Fig. 1(b-i)] for $0.4 < V < 600$ mm/s, despite the fact that the steady shear viscosities of samples A and B were in between those of the 30 and 60 wt.% PEG solutions. This surprising fact becomes more obvious in the case of sample C. Sample C did not wet the inner wall of the cylinder; however, the steady shear viscosity of sample C was much higher than that of the aqueous solution of PEG. A simple application of Eq. (1) with the shear viscosity shown in Fig. 2(a) cannot account for the absence of the film. Thus, we infer that samples A, B, and C exhibited the failure of film formation due to the appearance of an elastic behavior of the fluid.

TABLE II. Critical velocities for film formation.

Label	V_0 (mm/s)
15 wt.% PEG	220.3
30 wt.% PEG	46.0
60 wt.% PEG	2.7
A	
B	
C	

B. Rolling behavior of CTAB and NaSal solutions

In order to determine the mechanism responsible for the failure of film formation of viscoelastic fluids (CTAB and NaSal solutions), we conducted experiments with various samples having different G and τ values. The typical behavior of the fluid in the rotating cylinder changed, depending on the rotational velocity, as shown in Fig. 3 and in the videos in Ref. [26].

(i) *Film formation*. When the cylinder began to rotate at a low velocity (i.e., V was less than V_1), the contact line of the fluid moved with the same speed as that of the cylinder wall, leaving a thin fluid film behind. This corresponds to the film-forming regime known in the case of viscous fluids [1] [Fig. 1(b-ii)]. In this regime, the whole inner wall of the cylinder is wetted by the fluid: the top and bottom part are wetted by the fluid film and the fluid bump, respectively. The boundary of the two parts is steady.

(ii) *Steady rolling*. Above a certain critical velocity V_1, the thin film became unstable. When the cylinder began to rotate at a velocity slightly higher than V_1, the film formed initially but then detached from the cylinder wall. The detachment occurred in the following manner. At first, a certain part of the fluid film failed to move with the cylinder wall, and it caused

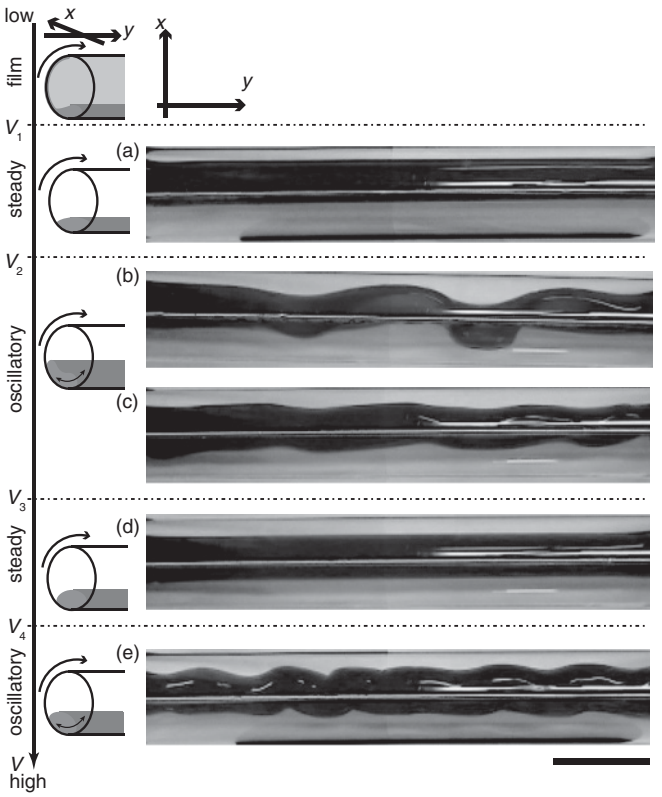

FIG. 3. Phase diagram of the motion of sample E. The vertical arrow represents the rotational velocity. The right-side diagrams are the snapshots of the sample in top view, where the top part of the snapshots corresponds to the rising inner wall. The scale bar corresponds to 80 mm. The rotational velocity V was (a) 5.93 mm/s, (b) 8.89 mm/s, (c) 76.56 mm/s, (d) 207.2 mm/s, and (e) 272.2 mm/s. The x axis is in the radial direction and the y axis is in the longitudinal direction of the cylinder. See also the corresponding videos in Ref. [26].

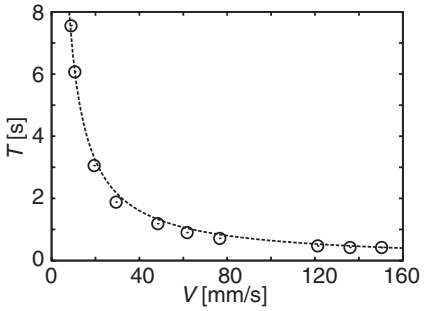

FIG. 4. Oscillation period of sample E for the region $V_2 < V < V_3$. The dotted line represents the fitting function $T = L/V$.

the formation of a fracture in the adjacent portion of the film. The propagation of the fracture caused the detachment.

As a result of the failure of the film formation, only the bottom of the cylinder was wetted by the fluid; i.e. only a fluid bump exists [Fig. 1(b-i)]. When the velocity was less than the second critical velocity V_2, the fluid bump exhibited steady rolling, where the shape of the fluid bump and the position of the contact line remained steady, as shown in Fig. 3(a).

(iii) *Oscillatory rolling*. Above the critical velocity V_2, the steady rolling of the fluid became unstable, and the shape of the fluid bump became wavy, as shown in Figs. 3(b) and 3(c). In this situation, the cross section of the fluid at an arbitrary position y repeated the cycle of climbing up the cylinder wall and slipping down to the bottom. The difference in the phase of the oscillation caused a wavy pattern, as shown in Figs. 3(b) and 3(c). Figure 4 shows the period T of oscillation as a function of the rotational velocity V. T decreased with increasing V and could be fitted as $T = L/V$. L was obtained as 64.2 mm, which approximately matched the width of the sample. Figure 5 shows the position x of the two contact lines (i.e., the two edges of the fluid bump) for a certain y in Fig. 3 as a function of time. It is seen that the pattern of the oscillation varied depending on the rotational velocity. For low velocity (close to V_2), the oscillation was triangular (slow climbing and quick falling), as shown in Fig. 5(a), while for high velocity (close to V_3) the oscillation became more sinusoidal, as shown in Fig. 5(b).

(iv) *Steady rolling*. Above the critical velocity V_3, the oscillation stopped and the fluid rolled at a fixed position near

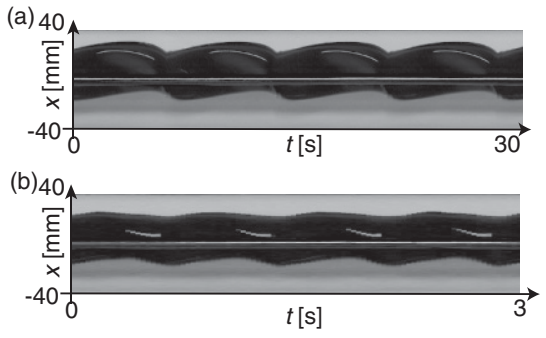

FIG. 5. Spatiotemporal diagram of the oscillatory behavior of sample E. The positions x of the contact line (i.e., the two edges of the fluid bump) for a certain point y in Fig. 3 are plotted against time, t. The rotational velocities were (a) 8.89 mm/s and (b) 76.56 mm/s.

TABLE III. Transition velocities of each sample. (*1) Film formation could not be observed even at the lowest rotational velocity. (*2) Instead of oscillation, fragments of the sample fluid began to adhere to the wall at high rotational velocity from a fluid bump, but no homogeneous film was observed. (*3) Reentry to the stable rolling regime could not be observed even at the highest rotational velocity of our apparatus.

Label	V_1 (mm/s)	V_2 (mm/s)	V_3 (mm/s)	V_4 (mm/s)
A	(*1)	(*2)		
B	(*1)	(*2)		
C	(*1)	304.0	(*3)	
D	(*1)	138.0	220.4	340.5
E	2.26	6.94	160.2	234.9
F	0.87	8.40	156.4	216.9
G	2.02	24.80	179.5	229.9
H	1.63	7.64	169.7	216.6
I	3.36	22.65	211.6	254.3
J	3.13	9.57	215.6	254.4

the bottom of the cylinder [Fig. 3(d)]. The cross section of the fluid seemed to be more circular than the one observed in the other low-velocity steady rolling region, $V_1 < V < V_2$.

(v) Unsteady rolling. With a further increase in the velocity, above V_4, the fluid began to oscillate again [Fig. 3(e)], but this oscillation may have been caused by a slight misalignment of the rotation axis of the cylinder and was ignored in our study.

These same behaviors were observed for the other samples. The observed transition velocities are listed in Table III. With samples A, B, C, and D, only the fluid bump was observed and the film region did not appear even at the lowest rotational velocity of our apparatus, 0.4 mm/s. We assume that the V_1 for these samples are smaller than 0.4 mm/s.

IV. DISCUSSION

We have seen that an aqueous solution of CTAB and NaSal placed at the bottom of a rotating cylinder exhibits very different behavior from a typical viscous fluid. In a typical viscous fluid, it is known that a fluid film is formed on the cylinder surface above V_0, as shown in Eq. (1). It is also known that the thickness of the film increases monotonically with increasing rotational velocity [27–31]. On the other hand, a fluid film disappears at the characteristic velocity V_1 for the CTAB and NaSal solution and only a bump of fluid rolls at the bottom of the cylinder for $V > V_1$. Here, we try to demonstrate the mechanism responsible for the failure of film formation and estimate the characteristic velocity, V_1.

In order to understand the reason for the failure of film formation, we focus on the junction between the film and the bump [Fig. 6(a)], given that the shear rate is maximum in this region. As the shear rate exceeds the inverse of the viscoelastic relaxation time of the sample $1/\tau$, the region becomes elastic and stress is accumulated in the region as the wall moves. If the elastic behavior persists, film formation fails due to the generation of a fracture, as was often observed in the actual experiment. In fact, a Maxwell fluid with a single relaxation time has been reported to show extremely low fracture energy [32,33].

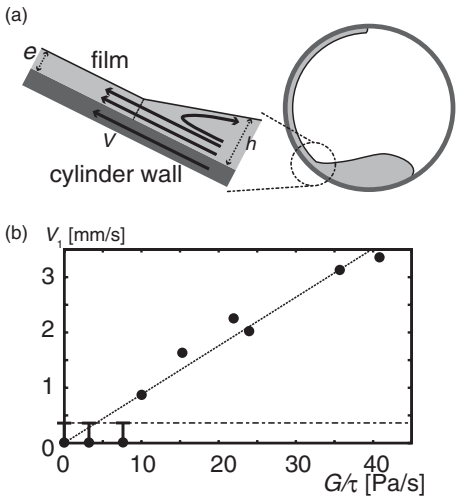

FIG. 6. (a) Schematic representation of the junction between the film and the bump. h and e represent the thickness of the sample and the film, respectively. (b) Experimentally obtained value of the critical velocity V_1 where film formation fails. The horizontal dotted line represents the lower limit of the rotational velocity of the apparatus. The filled circles represent the experimental data. V_1 of samples with small G/τ could not be seen due to limitations in the rotational velocity and are represented by the filled circles with a bar. The line is the linear fitting of the results using the fitting parameter described in the text.

The shear rate in the bump increases while approaching the film region because the thickness of the bump becomes smaller. Thus, the maximum shear rate in the system can be estimated by

$$\dot{\gamma}_{\max} \sim \frac{V}{e}, \tag{2}$$

where e is the thickness of the film.

We assume that the film fails when $\dot{\gamma}_{\max}$ exceeds the inverse of the viscoelastic relaxation time of the sample $1/\tau$. Thus, the critical velocity V_1 for film failure can be obtained from $\dot{\gamma}_{\max} \sim 1/\tau$; i.e.,

$$V_1 \sim \frac{e}{\tau}. \tag{3}$$

The thickness of the film e can be estimated by Derjaguin's law [28] because the film region behaves as a viscous liquid. Derjaguin's law states

$$e \sim \sqrt{\frac{G\tau V}{\rho g}}, \tag{4}$$

where we used the relation $\eta \sim G\tau$. Using Eqs. (3) and (4), we obtain

$$V_1 \sim \frac{G}{\rho g \tau}. \tag{5}$$

Figure 6(b) shows a comparison of the experimentally obtained critical velocities for film failure. The experimental results show that V_1 is indeed proportional to G/τ. The obtained slope is 8.5×10^{-5} m^3/N, which is in the same order as $1/\rho g \sim 1.0 \times 10^{-4}$ m^3/N.

Application of Derjaguin's law for the film region is justified by the following argument. Because the film follows the cylinder wall, the fluid in the film experiences a lower shear rate and behaves like a viscous liquid. The capillary number $\mathrm{Ca} = \eta V/\sigma$ in this region is approximately obtained as

$$\mathrm{Ca} = \frac{G\tau V}{\sigma} \sim \frac{10^2\ \mathrm{Pa\,s} \times 10^{-3}\ \mathrm{m/s}}{10^{-2}\ \mathrm{N/m}} \sim 10, \tag{6}$$

where σ is the surface tension of the sample and its order is estimated as 10^{-2} N/m. Here we also used the relation $\eta \sim G\tau$. It is known that Derjaguin's law applies to the film of a viscous liquid with such a large capillary number [28]. We believe that the detailed measurements of film thickness strongly support our theoretical prediction, and future studies should consider such measurements.

Interestingly, V_1 defined by Eq. (5) is independent of the critical velocity V_0 defined by Eq. (1), and can be smaller than V_0. In such a situation, the sample cannot wet the inner wall of the cylinder at any value of rotational velocity V. Thus, we can consider the condition for a dynamically nonwetting viscoelastic fluid from the condition $V_1 < V_0$ as

$$G < \sqrt{\frac{\rho g \sigma \theta_E^3}{9\sqrt{3}l}}. \tag{7}$$

This can also be written as

$$\tau > \eta \sqrt{\frac{9\sqrt{3}l}{\rho g \sigma \theta_E^3}}. \tag{8}$$

If the above condition is satisfied, the fluid cannot coat the substrate through the balance of gravitational force and the viscous force; i.e., dip coating cannot be achieved under such conditions.

The appearance of oscillatory rolling is another interesting feature indicated by our experimental results. The appearance of oscillation of the bump has been studied previously for viscous fluids, both from experiments [18,20] and theory [21,34]. In these reports, temporal oscillation as well as spatial wave formation of the bump have been reported. Reentry to the steady rolling regime by increasing rotational velocity has also been observed [20]. The critical difference between our results and those reports is that the film region always exists with the bump in the case of viscous fluids. In our experiment, for viscoelastic fluids, the film region disappears once the velocity exceeds V_1. The instability, temporal oscillation, and wave propagation are apparently amplified by the elastic nature of the sample fluids. In fact, the fluid bump rolled in the cylinder as if it were elastic material, as represented by the oscillation period $T = L/V$, where L is the width of the ribbon-shaped fluid bump. Thus, these phenomena can be related to the debonding process in elastic adhesives [11–14]. A detailed study on these instabilities, as well as transient behaviors, remains to be performed in the future.

V. CONCLUSION

In this study, we examined the dynamics of a viscoelastic Maxwell fluid confined in a rotating cylinder. At low rotational velocity, the behavior of our sample is similar to a viscous fluid;

i.e., the fluid film is observed together with the fluid bump at the bottom of a cylinder. Our sample shows a clear difference from a viscous fluid with the increase in the rotational velocity; i.e., the fluid film disappeared. The failure of film formation is caused by the appearance of elastic behavior and subsequent fracture formation at the boundary between the film and the bump, where the shear rate takes the maximum value. Furthermore, our study indicates the condition required for dynamically nonwetting behavior to be exhibited, because of which dip coating cannot be achieved. This result points to the importance of the interplay between bulk rheology and wetting behavior.

ACKNOWLEDGMENTS

Y.S. and H.S. contributed equally to this study. The authors would like to thank M. Kawabata and H. Sato for their helpful technical advice on constructing the experimental apparatus. We also would like to acknowledge Y. Tanaka (Yokohama Natl. Univ.) for inspiring discussion. Y.S. acknowledges support from a Grant-in-Aid for Research Activity Start-up (No. 23840019). T.K. received support from a JSPS Postdoctoral Fellowship for Research Abroad (No. 22-120) from MEXT, Japan. This work was supported in part by a Grant-in-Aid for Scientific Research (A) (No. 20244067).

[1] P. G. de Gennes, F. Brochard, and D. Quéré, *Capillarity and Wetting Phenomena Drops, Bubbles, Pearls, Waves* (Springer-Verlag, Berlin, 2004).
[2] P. G. de Gennes, Rev. Mod. Phys. **57**, 827 (1985).
[3] D. Bonn, J. Eggers, J. Indekeu, J. Meunier, and E. Rolley, Rev. Mod. Phys. **81**, 739 (2009).
[4] R. Hewson, N. Kapur, and P. Gaskell, J. Non-Newtonian Fluid Mech. **162**, 21 (2009).
[5] F. Kamisli, Chem. Eng. Process. **42**, 569 (2003).
[6] Y. Wei, E. Rame, L. M. Walker, and S. Garoff, J. Phys.: Condens. Matter **21**, 464126 (2009).
[7] M. Banaha, A. Daerr, and L. Limat, Eur. Phys. J. - Special Topics **166**, 185 (2009).
[8] T. Podgorski, J.-M. Flesselles, and L. Limat, Phys. Rev. Lett. **87**, 036102 (2001).
[9] E. Rio, A. Daerr, B. Andreotti, and L. Limat, Phys. Rev. Lett. **94**, 024503 (2005).
[10] H. Morita, S. Plog, T. Kajiya, and M. Doi, J. Phys. Soc. Jpn. **78**, 014804 (2009).
[11] C. Creton, J. Hooker, and K. R. Shull, Langmuir **17**, 4948 (2001).
[12] J. Sarkar, A. Sharma, and V. Shenoy, Langmuir **21**, 1457 (2005).
[13] T. Yamaguchi, K. Koike, and M. Doi, Europhys. Lett. **77**, 64002 (2007).
[14] J. Sarkar and A. Sharma, Langmuir **26**, 8464 (2010).
[15] M. A. Spaid and G. M. Homsy, Phys. Fluids **8**, 460 (1996).
[16] M. A. Spaid and G. M. Homsy, Phys. Fluids **9**, 823 (1997).
[17] A. Boudaoud, Eur. Phys. J. E **22**, 107 (2007).
[18] R. T. Balmer, Nature (London) **227**, 600 (1970).
[19] S. T. Thoroddsen and L. Mahadevan, Phys. Fluids **8**, S10 (1996).
[20] S. T. Thoroddsen and L. Mahadevan, Exp. Fluids **23**, 1 (1997).
[21] A. E. Hosoi and L. Mahadevan, Phys. Fluids **11**, 97 (1999).
[22] T. Shikata, H. Hirata, and T. Kotaka, Langmuir **3**, 1081 (1987).
[23] T. Shikata, H. Hirata, and T. Kotaka, Langmuir **4**, 354 (1988).
[24] Y. Hu, C. V. Rajaram, S. Q. Wang, and A. M. Jamieson, Langmuir **10**, 80 (1994).
[25] T. Inoue, Y. Inoue, and H. Watanabe, Langmuir **21**, 1201 (2005).
[26] See Supplemental Material at http://link.aps.org/supplemental/10.1103/PhysRevE.85.046307 for movies of experimental results.
[27] L. Landau and B. Levich, Acta Physicochim. USSR **17**, 42 (1942).
[28] B. V. Derjaguin, Acta Physicochim. USSR **20**, 349 (1943).
[29] J. Eggers, Phys. Rev. Lett. **93**, 094502 (2004).
[30] C. G. Ngan and E. B. Dussan, J. Fluid Mech. **118**, 27 (1982).
[31] F. Brochard-Wyart and P. G. de Gennes, Adv. Colloid Interface Sci. **39**, 1 (1992).
[32] J. R. Gladden and A. Belmonte, Phys. Rev. Lett. **98**, 224501 (2007).
[33] H. Tabuteau, S. Mora, G. Porte, M. Abkarian, and C. Ligoure, Phys. Rev. Lett. **102**, 155501 (2009).
[34] D. P. Vallette, W. S. Edwards, and J. P. Gollub, Phys. Rev. E **49**, R4783 (1994).